

In-hoc Concept Representations to Regularise Deep Learning in Medical Imaging

Valentina Corbetta^{*1,2,3} Floris Six Dijkstra^{*1,4} Regina Beets-Tan^{1,3} Hoel Kervadec^{4,5}
Kristoffer Wickstrøm⁶ Wilson Silva^{1,2}

¹The Netherlands Cancer Institute, The Netherlands ²Utrecht University, The Netherlands ³Maastricht University, The Netherlands

⁴University of Amsterdam, The Netherlands ⁵Amsterdam UMC, The Netherlands ⁶UiT The Arctic University of Norway, Norway
{v.corbetta, r.beetstan}@nki.nl, floris.six.dijkstra@student.uva.nl, h.t.g.kervadec@uva.nl,
kristoffer.k.wickstrom@uit.no, w.j.dossantossilva@uu.nl

Abstract

Deep learning models in medical imaging often achieve strong in-distribution performance but struggle to generalise under distribution shifts, frequently relying on spurious correlations instead of clinically meaningful features. We introduce LCRReg, a novel regularisation approach that leverages Latent Concept Representations (LCRs) (e.g., Concept Activation Vectors (CAVs)) to guide models toward semantically grounded representations. LCRReg requires no concept labels in the main training set and instead uses a small auxiliary dataset to synthesise high-quality, disentangled concept examples. We extract LCRs for predefined relevant features, and incorporate a regularisation term that guides a Convolutional Neural Network (CNN) to activate within latent subspaces associated with those concepts. We evaluate LCRReg across synthetic and real-world medical tasks. On a controlled toy dataset, it significantly improves robustness to injected spurious correlations and remains effective even in multi-concept and multiclass settings. On the diabetic retinopathy binary classification task, LCRReg enhances performance under both synthetic spurious perturbations and out-of-distribution (OOD) generalisation. Compared to baselines, including multitask learning, linear probing, and post-hoc concept-based models, LCRReg offers a lightweight, architecture-agnostic strategy for improving model robustness without requiring dense concept supervision. Code is available at this [link](#).

1. Introduction

Deep Learning (DL) has driven impressive advance in computer vision and medical image analysis, achieving expert-level performance on tasks such as object classification, le-

sion detection, and disease diagnosis [5, 11]. However, real-world deployment of these models remains limited due to their lack of robustness, particularly in the presence of domain shifts and spurious correlations [13, 22]. In clinical practice, data often comes from varied acquisition settings, institutions, and populations, which can cause critical shifts in distribution. At the same time, training datasets may contain spurious correlations, i.e., features that are statistically predictive but clinically irrelevant, that models can rely on, leading to degraded performance when those correlations break [29].

Improving robustness to such phenomena is essential for safe and reliable medical Artificial Intelligence (AI) [20, 28]. Traditional techniques such as data augmentation, domain adaptation, and adversarial training provide partial solutions, but have critical limitations. Data augmentation may not sufficiently simulate the full range of distributional variability encountered at test time [30]. Domain adaptation approaches often rely on access to unlabelled or partially labelled target-domain data, which is not always available in real-world clinical deployment settings [17]. Furthermore, adversarial training, while helpful for local robustness, does not distinguish between spurious and meaningful features, and may over-regularise and harm performance on unperturbed data, failing to suppress spurious correlations that are invariant to small perturbations [2]. As noted in recent surveys [19, 32], these assumptions severely constrain the generalisability and practical utility of these methods in healthcare applications.

An emerging alternative strategy is to constrain models to rely on semantically meaningful features, such as expert-defined medical concepts. The motivation is that models grounded in medically relevant features are less likely to rely on spurious correlations and more likely to generalise across domains. Several recent works support this direction. For example, Concept Whitening (CW) aligns latent

^{*}Equal contribution

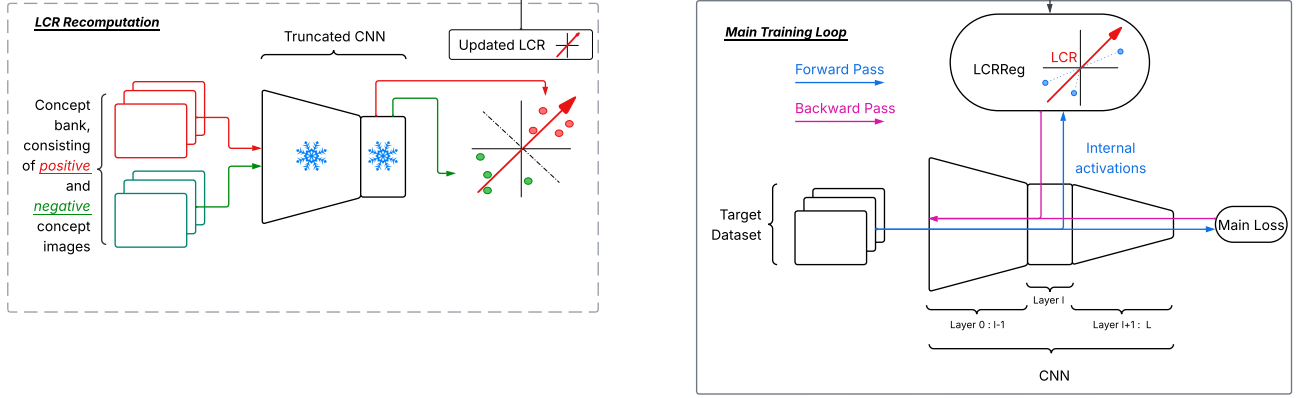


Figure 1. Illustration of the proposed LCRReg. The main training loop optimises a CNN using the $\mathcal{L}_{MainLoss}$ and a weighted Latent Concept Representation (LCR) Loss (\mathcal{L}_{LCRReg}). At the start of each recomputation interval I_{rec} , LCR recomputation is executed: concept images from the concept bank are passed through the truncated CNN to compute updated LCRs based on intermediate activations. These LCRs are then used for regularisation in subsequent training steps.

features with axes corresponding to predefined concepts [4], and MICA integrates multi-level concept supervision to enhance robustness and interpretability [3]. Class Artifact Compensation (CIArC) suppresses spurious dependencies by projecting representations away from known artifact directions [2]. By contrast, Post-hoc Concept Bottleneck Model (PCBM) uses Concept Activation Vectors (CAVs) for test-time interpretability, and its variant Hybrid Post-hoc Concept Bottleneck Model (PCBM-h) then applies a separate residual-fitting step to recover any predictive signal the CAVs themselves miss [33]. Notably, these methods usually require dense concept supervision throughout the training dataset or rely on modifying the model architecture, limiting their scalability.

In this work, we pursue a general and scalable version of this concept-regularisation strategy. We introduce LCR Regularization (LCRReg), which leverages Latent Concept Representations (LCRs), i.e., post-hoc vectors that describe directions or regions in the model’s activation space corresponding to clinically meaningful concepts. Examples include CAVs [15], pattern-CAVs [26], Regression Concept Vectors (RCVs) [9], and Concept Activation Regions (CARs) [6]. Unlike prior works that use LCRs purely for explanation, we incorporate them directly into training as a form of semantic regularisation. Through a regularisation loss that encourages alignment with concept subspaces or separation from spurious ones, we guide the model to encode more robust, clinically grounded representations.

Our contributions are the following:

- **Concept-based regularisation for robustness:** We propose LCRReg, a method that improves robustness to spurious correlations and out-of-distribution (OOD) shifts by aligning intermediate representations with clinically

meaningful concept directions.

- **Training without paired concept-image labels:** Our method only requires concept annotations in a small auxiliary dataset and does not rely on concept supervision in the main training set, making it scalable and practical.
- **Systematic comparison of LCR types and losses:** We evaluate multiple concept representation methods (CAVs, pattern-CAVs, RCVs, CARs and regularisation strategies (subspace alignment, decision-boundary distance) in terms of their robustness effects.
- **Robustness evaluation across tasks and datasets:** We demonstrate improved performance under distribution shifts, including synthetic spurious correlations and OOD benchmarks, on a toy dataset, namely Elements [24], and the medical imaging task of Diabetic Retinopathy (DR) classification.

2. Methodology

Given a Neural Network (NN)

$$\mathcal{N} : \mathbb{R}^{d_0} \rightarrow \mathbb{R}^{d_L}, \quad (1)$$

where d_0 is the dimensionality of the input, and d_L is the number of output units (i.e., the pre-softmax logits for each of the d_L classes), we augment its standard training loss with a regularisation term LCRReg that aligns internal representations with directions associated with clinically meaningful concepts:

$$\mathcal{L}_{total} = \beta_t \cdot \mathcal{L}_{MainLoss} + \alpha_t \cdot \mathcal{L}_{LCRReg} \quad (2)$$

Here, $\mathcal{L}_{MainLoss}$ is the classification objective function, in our case the standard Cross-Entropy (CE) loss, and β_t and α_t respectively weigh the relative contribution of the

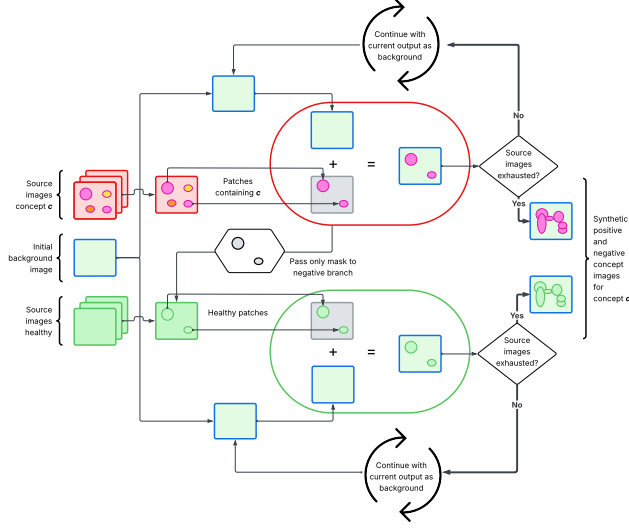


Figure 2. Overview of the concept creation pipeline. Positive samples are generated by pasting patches containing concept c onto healthy images. Negative samples are created similarly, using only healthy tissue patches. This ensures both image types are synthetic and differ mainly in the presence of the concept.

classification loss and of the regularisation term. The concept directions are derived from an auxiliary dataset of K predefined concepts, $C = \{c_{1,l}, c_{2,l}, \dots, c_{K,l}\}$ and used to compute regularisation losses over layer $l \in T$, where T is a set of selected target layers. Figure 1 depicts an overview of the proposed approach.

In this Section, we present the components of our method in detail, including:

- The process for constructing the concept dataset C .
- The different types of LCRs we evaluate.
- The alternative formulations of the regularisation loss.
- The training procedures used to integrate regularisation into learning.

2.1. Concept Creation

Creating high-quality, disentangled concept representations is a key prerequisite of our regularisation strategy. In natural image settings, such concepts are often visually distinct and easily annotated (e.g., “striped”, “red”). However, in medical imaging, clinically relevant features are typically subtle, domain-specific and difficult to label, requiring expert-level pixel-wise annotations. These annotations are expensive and time-consuming to obtain, making scalable concept-based training particularly challenging. Additionally, while automated concept extraction methods exist [25], their applicability in medical imaging remains limited due to the subtlety and domain specificity of relevant features [12]. Moreover, a key challenge lies in avoiding concept entanglement, i.e., the presence of multiple overlapping or correlated features within the same sample. Con-

cept entanglement occurs when samples labelled as positive for a concept also contain features associated with other concepts (e.g., lesions often co-occur with artifacts or vessel abnormalities). If such co-occurrence is not controlled, the learnt LCRs may reflect a mix of concepts rather than isolating the intended one, undermining both robustness and interpretability. A more detailed explanation of this problem and a visual example of concept entanglement in DR can be found in Appendix A.

To address both the scarcity of expert annotations and the risk of entangled concept signals, we design a modular concept synthesis pipeline that requires only a small number of annotated images, and systematically generates disentangled concept examples; this ensures that the only distinguishing factor between positive and negative samples is the presence or absence of the target concept.

The pipeline, illustrated in Figure 2, builds a synthetic concept bank through compositional editing as follows:

1. We start from a set of healthy background images \mathcal{H} , which are free of all target concepts.
2. For each target concept c , we collect a set of annotated source images \mathcal{S} , each paired with a binary segmentation mask $m_{c,k}$ identifying the concept’s location.
3. For each background image $h_b \in \mathcal{H}$ and for each target concept c , we generate synthetic concept examples through N iterative modifications:
 - (a) We initialise the image with $x_0 = h_b$.
 - (b) For $i = 1, \dots, N$:
 - i. We select a source image $p \in \mathcal{S}$ and we extract the concept-specific mask m .
 - ii. To generate a positive image, we paste the extracted concept patches from p onto x_{i-1} to create x_i^+ .
 - iii. To generate a negative image, we sample a different healthy image $h_s \in \mathcal{H} : h_s \neq h_b$. We then extract a patch from a region spatially located on h_s as m on p and we paste them onto x_{i-1} to create x_i^- .

N is a hyperparameter that controls how many different concept instances are inserted per synthetic sample. Increasing N produces more densely composed examples, reinforcing the concept signal but potentially increasing visual artificiality. Conversely, a smaller N yields more natural images at the cost of weaker signal. This trade-off lets us control the intensity and variability of concept presence across the dataset.

We extend this approach to continuous-valued concepts, e.g., for regression-based LCRs like RCVs. In this instance, we synthesise only positive samples and assign each a scalar score based on the proportion of pixels occupied by the concept, enabling the model to learn a continuous representation of concept strength.

Once computed, the LCRs can be reused throughout

training, making the pipeline highly annotation-efficient. While our method is designed to be general and transferable across medical tasks and modalities, its practical applicability may vary depending on concept granularity, segmentation quality, and clinical interpretability. Nonetheless, it provides a strong and scalable foundation for concept-based regularisation with minimal concept annotation.

2.2. Latent Concept Representations (LCRs)

As mentioned in Section 1, we consider four different LCR methods for regularisation that can be plugged into our regularisation loss.

- Filter-CAVs [15] leverage a binary classifier, e.g., a Support Vector Machine (SVM), that learns to separate positive and negative concept examples in the activation space; the normal vector of the resulting Decision Boundary (DB) defines the concept.
- Pattern-CAVs [26] define concept vectors as the direction between the class-conditional means of neural activations for concept-positive and concept-negative samples. Unlike filter-CAVs, which rely on training a classifier, pattern-CAVs compute this direction directly.
- CARs [6] improve filter-CAVs by extending the underlying classifier to a non-linear kernel for binary classification.
- RCVs [9] extend filter-CAVs to use ordinal labels, by transforming the problem from binary classification to ordinal regression; an example, instead of being labelled positive or negative, is assigned a numerical value as a measure of how strongly the concept is represented in the input image.

2.3. Concept-based Regularisation

We describe two variants of LCRReg, based on the nature of the concept representation: one based on distances to concept subspaces (for vectorial LCRs), and one based on distances from learnt DBs (for classifier-based LCRs).

2.3.1. Notation

Let $\mathcal{N}_l(x) \in \mathbb{R}^{d_l}$ denote the activation of the network at layer $l \in T$. Let $\{v_{1,l}, v_{2,l}, \dots, v_{K,l}\}$ be concept vectors derived from C at layer l . These vectors define the concept subspace $\mathcal{C}_l = \text{span}(v_{1,l}, v_{2,l}, \dots, v_{K,l}) \subset \mathbb{R}^{d_l}$. We denote the orthogonal projection of an activation $\mathcal{N}_l(x)$ onto \mathcal{C}_l by $\hat{\mathcal{N}}_l(x) = \Pi_{\mathcal{C}_l}(\mathcal{N}_l(x))$. We use $D(\cdot, \cdot)$ to represent a generic distance function.

Subspace-based Regularisation For linear concept representations (e.g., filter-CAVs, pattern-CAVs, and RCVs), we define the subspace-based regularisation loss as

$$\mathcal{L}_{LCRReg}^{Sub} = \frac{1}{|T|} \sum_{l \in T} D(\mathcal{N}_l(x), \Pi_{\mathcal{C}_l}(\mathcal{N}_l(x))) \quad (3)$$

By adopting the cosine distance:

$$D^{cos}(\mathcal{N}_l(x), \mathcal{C}_l) = 1 - \frac{\langle \mathcal{N}_l(x), \hat{\mathcal{N}}_l(x) \rangle}{\|\mathcal{N}_l(x)\|_2 \cdot \|\hat{\mathcal{N}}_l(x)\|_2 + \epsilon} \quad (4)$$

with $\epsilon \approx 10^{-8}$, added for numerical stability. The cosine distance is bounded between 0 and 1, thus encouraging stable optimisation. It promotes alignment with the concept subspace without driving activation norms toward zero, a common side effect of the alternative unbounded norm-based distance.

2.4. Decision Boundary-based Regularisation

When concepts are represented via learnt classifiers (e.g., filter-CAVs or CARs), we apply a different loss that penalises activations lying close to the learnt DBs.

Let $\phi_{i,l} : \mathbb{R}^{d_l} \rightarrow \mathbb{R}$ be the decision function for concept i at layer l , which outputs the signed distance of the activation to the decision boundary. To model diminishing sensitivity to large distances, we apply a monotonically decreasing transformation $G : \mathbb{R} \rightarrow \mathbb{R}$. The resulting loss penalises activations closer to any DB more strongly and yields the following formulation:

$$\mathcal{L}_{LCRReg}^{DB} = -\frac{1}{|T| \cdot K} \sum_{l \in T} \sum_{i=1}^K |G(\phi_{i,l}(\mathcal{N}_l(x)))| \quad (5)$$

In our experiments, we use an exponential decay function $G(d) = \exp(-d/c)$ with hyperparameter $c > 0$ controlling the rate of the decay, which smoothly increases the penalty for activations lying near the DB.

2.5. Training Strategies

Effectively combining concept-based supervision with primary task learning requires careful consideration of two key elements: first, how the relative weight of the regularisation signal evolves during training; second, how often the LCRs are recomputed. Improper handling of either can result in underutilised supervision, unstable optimisation, or information leakage.

2.5.1. Regularisation Scheduling

Rather than fixing the balance between the classification loss and regularisation throughout training, we explore different scheduling schemes for the loss weights α_t and β_t . These define how strongly concept signals influence learning over time. We consider three strategies:

- Static regularisation: the simplest approach, where $\beta_t = 1$ and α_t is kept at a constant value, obtained via optimisation. To allow the network to learn useful features before regularisation begins, we optionally delay its activation by setting $\alpha_t = 0$ for $t < \hat{t}$, where \hat{t} is a schedule hyperparameter.

- **Dynamic regularisation:** α_t is increased and β_t is decreased over training. This schedule assumes that LCRs may be more accurate at later stages, when internal features are more meaningful. When the regularisation strength α_t increases toward the end of training, the model relies more heavily on the concept representations. This can help override signals from spurious correlations. As a result, the model may become more robust and aligned with clinically meaningful features. However, this approach introduces additional hyperparameters, resulting in a more complex training setup compared to static regularisation.
- **3-stage training:** to isolate learning signals and avoid mutual interference, we adopt a staged training strategy:
 1. Stage I: train the model with only the classification loss $\mathcal{L}_{MainLoss}$ ($\beta_t = 1, \alpha_t = 0$).
 2. Stage II: switch to concept regularisation only ($\beta_t = 0, \alpha_t = 1$).
 3. Stage III: fine-tune only layers on top of the LCR target layers with the classification loss ($\beta_t = 1, \alpha_t = 0$), freezing the rest of the network.

The motivation behind the staged training setup is twofold:

- To reduce information leakage. When concept supervision and task supervision are applied simultaneously, the model may learn to satisfy both objectives by encoding shortcuts or spurious correlations that happen to co-occur with the target concepts. NNs are flexible enough to exploit such correlations, especially early in training when internal representations are still forming. By isolating the concept supervision phase (Stage II), we reduce gradient propagation beyond target layers, limiting the model’s ability to track spurious correlations across the entire network. This encourages internal representations to align more cleanly with the intended concept subspaces, rather than entangled or confounded features.
- To enable investigative comparison. The staged design also allows us to explicitly assess the value of incorporating concept supervision during feature learning: if training with LCRReg in Stage II leads to a better final performance than applying them only post-hoc, this provides evidence that our method actively shapes internal representations in a beneficial way.

2.5.2. LCR Recomputation Interval

Unlike post-hoc interpretability settings where LCRs are computed only once, regularisation requires integrating them into the training loop. However, since model weights evolve during training, a concept vector computed once may become outdated. We define a recomputation interval I_{rec} to control how frequently LCRs are updated.

At one extreme, we recompute after every training epoch, which maximises alignment with the current model



Figure 3. Sample images from the Elements dataset.

but introduces high computational overhead and training instability due to the moving objective. At the other extreme, recomputing only once at the beginning improves stability but may result in misaligned supervision.

In Section 3, we investigate the effect of the presented training strategies.

3. Experiments

We evaluate our proposed method, LCRReg, in two complementary settings: a controlled synthetic dataset, Elements, and a real-world medical imaging task, namely DR classification.

3.1. Synthetic Experiments

We first validate LCRReg on the synthetic Elements dataset, explicitly designed to control the presence of concepts and spurious correlations. Each image comprises distinct “elements” described by five attributes: shape, colour, texture, location, and size (examples are reported in Figure 3). We initially focus on a binary classification task: detecting squares. During training, squares consistently have a spurious correlation, diagonal stripes, that is absent in the test set. The dataset consists of 300 training images and 1000 images each for validation and testing. We train ResNet18 [10] pretrained on ImageNet [7] for 20 epochs using the Adam optimiser [16] with a learning rate of 10^{-5} and weight decay of 10^{-4} and report Balanced Accuracy (BA). We apply LCRReg to the 1×1 projection convolution that adjusts the residual connection in the first module of the last ResNet block.

3.1.1. Ablation on Hyperparameter Impact

We evaluate the impact of three key hyperparameters on the Elements dataset: LCRReg loss weight α_t , regularisation start epoch \tilde{t} , and LCR recomputation interval I_{rec} . Results (Figure 12 in Appendix B) show that performance improves with higher α_t and immediate regularisation ($\tilde{t} = 0$). Frequent LCR recomputation introduces instability, with best results achieved by computing concepts once at the start. These findings suggest that strong, early regularisation with fixed concept vectors is effective for simple settings.

3.1.2. Regularisation Scheme Comparison

We compare the three regularisation schemes introduced in Section 2: static, dynamic, and 3-stage training. Hyperparameters are optimised via Optuna [1] and evaluated statis-

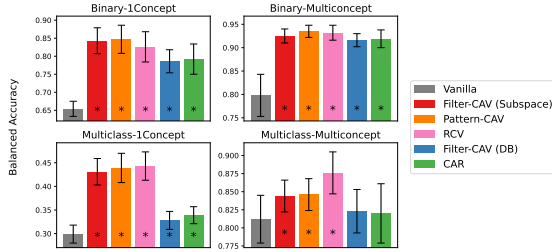


Figure 4. Balanced Accuracy (BA) of ResNet18 trained on a dataset that contains spurious correlations, and evaluated on a dataset without the correlation. Error bars indicate standard deviation over 20 runs, all on differently generated datasets. * indicates that the difference with the vanilla model is statistically significant at the 0.01 level, using a pairwise t-test.

tically over 15 dataset splits; detailed results of the optimisation are reported in Appendix B. Figure 13 in Appendix B shows no significant difference between static and dynamic schemes ($p = 0.76$). Static regularisation without LCR recomputation achieves the best overall performance. 3-stage training significantly underperforms ($p < 0.0001$).

3.1.3. Multi-concept and Multi-class settings

We extend our evaluation to assess robustness in more complex scenarios:

- Binary-multiconcept: detect two shapes simultaneously (squares and triangles).
- Multiclass-1concept: classify images based on the number of squares (classes 0-4).
- Multiclass-multiconcept: classify images based on the presence of squares, triangles and circles.

Because static regularisation uses the fewest hyperparameters and, as our optimisation search showed, performs on par with more complex setups, we employ LCRReg in this mode. Moreover, we employ the hyperparameters tuned on the Binary-1Concept task for all the settings. From Figure 4, we notice that LCRReg consistently outperforms the vanilla baseline (ResNet18 without LCRReg) across all settings. Cosine-based losses (Pattern-CAV, RCV) yield statistically significant improvements. DB-based methods are effective but slightly less so.

3.2. Diabetic Retinopathy Classification

We evaluate LCRReg on the clinical task of DR detection. Training uses the APTOS dataset [14], with the FGADR dataset [34] providing pixel-level annotations of microaneurysms, a concept signifying the arising of DR. To create the concepts for DR we follow the pipeline described in Section 2; example figures and more details can be found in Appendix A. We evaluate model robustness against artificially injected spurious correlations (synthetic visual markers, shown in Figure 5) and generalisation to OOD datasets.

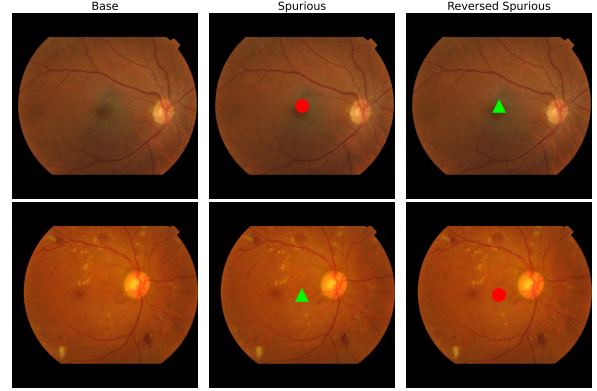


Figure 5. Example of spurious correlations on non-preprocessed images from APTOS. From left to right: the base images, with Spurious Correlations, with the Reversed Spurious Correlations.

3.2.1. Robustness to Spurious Correlations

We formulate DR as a binary classification (healthy vs. unhealthy) and artificially inject strong synthetic markers correlated with class labels during training. We evaluate robustness to three scenarios:

- Spurious dataset: the test set retains original spurious correlation distribution.
- Reversed spurious dataset: the spurious correlations are inverted (markers switched classes).
- Base dataset: original test set, without the artificial correlations.

Baselines. To contextualise our results, we compare LCRReg against several baselines:

- PCBM-h [33] projects activations onto a concept subspace defined by post-hoc CAVs and employs residual fitting to preserve accuracy. PCBM-h provides interpretability through concept alignment but does not explicitly regularise against spurious correlations.
- Multi-Task Learning (MTL) jointly trains the model on the primary classification task and an auxiliary task predicting concept presence. By explicitly supervising concepts during training, MTL may implicitly encourage reliance on clinically meaningful features.
- Linear probing is similar to MTL, but instead of placing the prediction head on top of the final features, it is attached to the intermediate ones, specifically in the same layer where LCRs are computed. This allows us to assess whether the LCR calculation pipeline is necessary or if we could simply add a linear classification layer on the features.

Training Setup and Hyperparameter Tuning. We evaluate models at different levels of spurious correlation pres-

Table 1. Out-of-Distribution performance in Balanced Accuracy (BA) (std) for vanilla and LCRReg models. Models were trained on APTOS via the same protocol, and evaluated on the entirety OOD datasets. Results are averaged over 5 runs.

Model	In-Distribution	Out-Of-Distribution					
	APTOS	RLDR	IDRiD	DEEPDR	DDR	EYEPACS	Avg
Vanilla	96.8 (2.1)	52.06 (1.83)	68.67 (6.46)	55.83 (2.60)	57.17 (3.96)	52.10 (0.01)	57.17
+LCRReg	94.7 (2.4)	51.75 (1.36)	69.48 (3.54)	58.33 (2.48)	59.70 (1.77)	52.31 (5.20)	58.31
PCBM-h	96.4 (1.8)	54.14 (2.10)	69.04 (6.03)	62.26 (3.72)	60.38 (3.81)	53.08 (0.01)	59.78
+ LCRReg	95.2 (3.1)	54.58 (2.26)	71.85 (8.80)	62.85 (4.08)	61.84 (2.85)	54.79 (1.68)	61.18

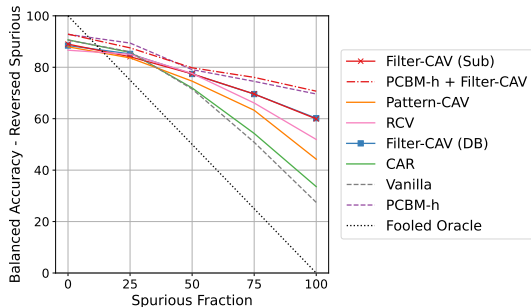


Figure 6. Performance averaged over 5 runs of the various LCRReg models, PCBM-h, and the vanilla model, assessed across multiple values of p_{SC} . Hyperparameters are tuned on the same data distribution of the training set.

ence, denoted as $p_{SC} \in \{0.00, 0.25, 0.50, 0.75, 1.00\}$, using a ResNet50 [10] backbone, pretrained on ImageNet.

Results are reported on a test set with reversed spurious correlations, averaged over 5 runs, and can be seen in detail in Appendix C. Hyperparameters tuned via Optuna on validation sets matching the training distribution yield minimal robustness improvement, as optimisation favours exploiting spurious cues. Among these tuned models, only PCBM-h demonstrates consistent robustness across varying p_{SC} levels, maintaining high predictive performance until spurious correlations dominate the entire training set ($p_{SC} = 1$).

Therefore, we select robust parameters derived from the synthetic experiments ($\alpha_t = 100$, $\tilde{t} = 0$, $I_{rec} = \infty$). These settings substantially improved robustness particularly on the reversed spurious dataset (Figure 6). LCRReg significantly outperforms the baseline models, with Filter-CAV achieving the best overall performance. Combining LCRReg with PCBM-h provides additional incremental robustness improvements, leveraging both regularisation during training and interpretability post-training.

Saliency map visualisations depicted in Figure 7 qualitatively confirm LCRReg reduces reliance on spurious correlations compared to the vanilla baseline.

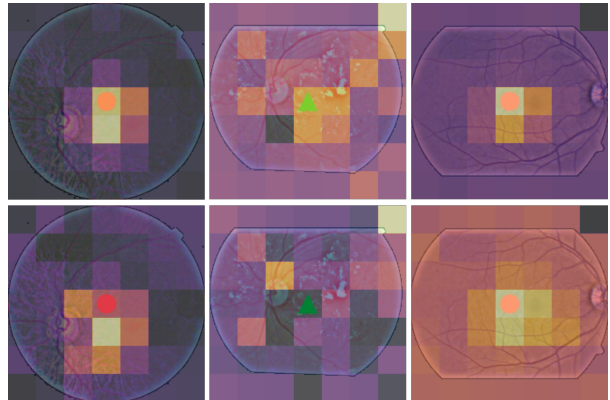


Figure 7. Example saliency map overlays from the vanilla model (top row) and the same model with LCRReg applied (bottom row). Each column corresponds to the same test image across models. Yellow indicates stronger activation; purple indicates weaker activation.

3.2.2. OOD Generalisation

We assess generalisation by training on APTOS and evaluating on five unseen datasets: RLDR [31], IDRiD [27], DEEPDR [21], DDR [18], and EYEPACS [8]. LCRReg achieves modest yet statistically significant improvements over the vanilla baseline and PCBM-h (Wilcoxon test, $p = 0.0058$), as can be seen from Table 1.

3.2.3. Ablation on Model Architectures

We evaluate LCRReg’s generalisability across different backbone models. Results reported in Table 2 in Appendix B confirm reduced reliance on spurious correlations, though the results are not statistically significant individually. Notably, the effect is minimal for ResNet152, suggesting that the current regularisation method is not yet sufficient to effectively address spurious correlations in larger architectures.

4. Discussion

Our results demonstrate that LCRReg, a plug-in regularisation method leveraging LCRs, can improve robustness

to spurious correlations in both synthetic and real-world medical image classification tasks. Compared to traditional methods requiring dense concept supervision, LCRReg operates without concept labels on the main dataset, using instead a lightweight synthetic concept bank generated via compositional editing. This improves scalability for real-world deployment.

In synthetic settings, LCRReg consistently improved robustness of the vanilla model across all experimental configurations. Performance gains were strongest in the Binary-1Concept task, where hyperparameters were tuned, but remained competitive even when the same parameters were reused in more complex multi-concept and multiclass settings. Notably, DB-based methods showed decreasing relative benefit as task complexity increased, suggesting that cosine-based subspace regularisation may generalise better in high-dimensional concept spaces.

In real-world experiments, LCRReg outperformed standard baselines, like multitask learning and linear probing. While PCBM-h remained the strongest stand-alone baseline under distribution shift, combining it with LCRReg offered modest additional robustness gains, highlighting the complementary strengths of regularisation during training and concept-based adjustments post hoc.

Among LCR types, filter-CAVs provided the most reliable robustness gains in the clinical setting, despite being less sophisticated than CARs or pattern-CAVs. This aligns with the hypothesis that discriminative directions, rather than descriptive activations, offer a stronger inductive bias when used for regularisation. Frequent LCR recomputation did not improve results; on the contrary, recomputing CAVs only once at the beginning yielded more stable and robust performance, likely due to avoiding moving-target dynamics during optimisation.

Hyperparameter tuning further revealed consistent trends: starting regularisation early and using a high regularisation weight (α_t) improved performance, especially for cosine-based loss formulations. However, tuning remains non-trivial in the presence of spurious correlations, as optimising on in-distribution validation sets often favours learning spurious cues. Future methods may benefit from tuning procedures guided by robustness-aware metrics or proxy OOD validation splits.

5. Conclusion

We introduce LCRReg, a scalable regularisation method that uses LCRs derived from synthetic concept images to guide model training toward semantically meaningful features. Our approach requires only minimal auxiliary supervision and can be easily integrated into existing architectures as a modular regularisation technique.

Experiments on both a controlled synthetic dataset and DR classification show that LCRReg improves robustness

to spurious correlations and provides modest gains in OOD generalisation. It outperforms more complex concept supervision baselines under the same constraints and shows complementary benefits when combined with post hoc approaches such as PCBM-h.

Despite its simplicity, filter-CAV remains the most effective LCR type, suggesting that separation-based concept vectors are particularly well-suited for regularisation. Our results also show that strong early regularisation with static concept vectors is a viable and stable training strategy. Surprisingly, we found that LCRReg performed best when the CAV was computed only once. While internal representations evolve during training, updating the CAVs too frequently introduced instability, likely due to the moving target problem. A promising solution may involve using a moving average of the CAV, enabling smoother updates and more stable training.

These findings underscore the potential of using concept-based signals for robustness without requiring extensive concept-label supervision. Future work may explore extending LCRReg to deeper models, multi-concept settings, and combining it with gradient manipulation techniques (e.g., Gradient Surgery [23]) to further improve training stability and scalability.

Acknowledgements

Research at the Netherlands Cancer Institute is supported by grants from the Dutch Cancer Society and the Dutch Ministry of Health, Welfare and Sport. Kristoffer Wickstrøm is financially supported by the Research Council of Norway, through its Center for Research-based Innovation funding scheme (grant no. 309439).

References

- [1] Takuya Akiba, Shotaro Sano, Toshihiko Yanase, Takeru Ohta, and Masanori Koyama. Optuna: A next-generation hyperparameter optimization framework. In *Proceedings of the 25th ACM SIGKDD international conference on knowledge discovery & data mining*, pages 2623–2631, 2019. 5
- [2] Christopher J. Anders, Leander Weber, David Neumann, Wojciech Samek, Klaus-Robert Müller, and Sebastian Lapuschkin. Finding and removing clever hans: Using explanation methods to debug and improve deep models, 2020. 1, 2
- [3] Yequan Bie, Luyang Luo, and Hao Chen. Mica: Towards explainable skin lesion diagnosis via multi-level image-concept alignment. In *Proceedings of the AAAI Conference on Artificial Intelligence*, pages 837–845, 2024. 2
- [4] Zhi Chen, Yijie Bei, and Cynthia Rudin. Concept whitening for interpretable image recognition. *Nature Machine Intelligence*, 2(12):772–782, 2020. 2
- [5] Shern Ping Choy, Byung Jin Kim, Alexandra Paolino, Wei Ren Tan, Sarah Man Lin Lim, Jessica Seo, Sze Ping Tan, Luc Francis, Teresa Tsakok, Michael Simpson, et al. Systematic review of deep learning image analyses for the diagnosis

- and monitoring of skin disease. *NPJ Digital Medicine*, 6(1): 180, 2023. 1
- [6] Jonathan Crabbé and Mihaela van der Schaar. Concept activation regions: A generalized framework for concept-based explanations. *Advances in Neural Information Processing Systems*, 35:2590–2607, 2022. 2, 4
- [7] Jia Deng, Wei Dong, Richard Socher, Li-Jia Li, Kai Li, and Li Fei-Fei. Imagenet: A large-scale hierarchical image database. In *2009 IEEE conference on computer vision and pattern recognition*, pages 248–255. Ieee, 2009. 5
- [8] Emma Dugas, Jared, Jorge, and Will Cukierski. Diabetic retinopathy detection. <https://kaggle.com/competitions/diabetic-retinopathy-detection>, 2015. Kaggle. 7
- [9] Mara Graziani, Vincent Andrearczyk, and Henning Müller. Regression concept vectors for bidirectional explanations in histopathology. In *Understanding and Interpreting Machine Learning in Medical Image Computing Applications: First International Workshops, MLCN 2018, DLF 2018, and iMIMIC 2018, Held in Conjunction with MICCAI 2018, Granada, Spain, September 16-20, 2018, Proceedings 1*, pages 124–132. Springer, 2018. 2, 4
- [10] Kaiming He, Xiangyu Zhang, Shaoqing Ren, and Jian Sun. Deep residual learning for image recognition. In *Proceedings of the IEEE conference on computer vision and pattern recognition*, pages 770–778, 2016. 5, 7
- [11] Shih-Cheng Huang, Anuj Pareek, Malte Jensen, Matthew P Lungren, Serena Yeung, and Akshay S Chaudhari. Self-supervised learning for medical image classification: a systematic review and implementation guidelines. *NPJ Digital Medicine*, 6(1):74, 2023. 1
- [12] Ta Duc Huy, Sen Kim Tran, Phan Nguyen, Nguyen Hoang Tran, Tran Bao Sam, Anton van den Hengel, Zhibin Liao, Johan W Verjans, Minh-Son To, and Vu Minh Hieu Phan. Interactive medical image analysis with concept-based similarity reasoning. In *Proceedings of the Computer Vision and Pattern Recognition Conference*, pages 30797–30806, 2025. 3
- [13] Dovile Juodelyte, Yucheng Lu, Amelia Jiménez-Sánchez, Sabrina Bottazzi, Enzo Ferrante, and Veronika Cheplygina. Source matters: Source dataset impact on model robustness in medical imaging. In *International Workshop on Applications of Medical AI*, pages 105–115. Springer, 2024. 1
- [14] Karthik, Maggie, and Sohier Dane. Aptos 2019 blindness detection. <https://kaggle.com/competitions/aptos2019-blindness-detection>, 2019. Kaggle. 6
- [15] Been Kim, Martin Wattenberg, Justin Gilmer, Carrie Cai, James Wexler, Fernanda Viegas, et al. Interpretability beyond feature attribution: Quantitative testing with concept activation vectors (tcav). In *International conference on machine learning*, pages 2668–2677. PMLR, 2018. 2, 4, 11
- [16] Diederik P Kingma. Adam: A method for stochastic optimization. *arXiv preprint arXiv:1412.6980*, 2014. 5
- [17] Hualing Li, Yaodan Wang, and Yan Qiang. A semi-supervised domain adaptive medical image segmentation method based on dual-level multi-scale alignment. *Scientific Reports*, 15(1):8784, 2025. 1
- [18] Tao Li, Yingqi Gao, Kai Wang, Song Guo, Hanruo Liu, and Hong Kang. Diagnostic assessment of deep learning algorithms for diabetic retinopathy screening. *Information Sciences*, 501:511 – 522, 2019. 7
- [19] Jian Liang, Ran He, and Tieniu Tan. A comprehensive survey on test-time adaptation under distribution shifts. *International Journal of Computer Vision*, 133(1):31–64, 2025. 1
- [20] Geert Litjens, Thijs Kooi, Babak Ehteshami Bejnordi, Arnaud Arindra Adiyoso Setio, Francesco Ciompi, Mohsen Ghafoorian, Jeroen Awm Van Der Laak, Bram Van Ginneken, and Clara I Sánchez. A survey on deep learning in medical image analysis. *Medical image analysis*, 42:60–88, 2017. 1
- [21] Ruhan Liu, Xiangning Wang, Qiang Wu, Ling Dai, Xi Fang, Tao Yan, Jaemin Son, Shiqi Tang, Jiang Li, Zijian Gao, Adrian Galdran, J.M. Poorneshwaran, Hao Liu, Jie Wang, Yerui Chen, Prasanna Porwal, Gavin Siew Wei Tan, Xi-aokang Yang, Chao Dai, Haitao Song, Mingang Chen, Huating Li, Weiping Jia, Dinggang Shen, Bin Sheng, and Ping Zhang. Deepdrd: Diabetic retinopathy—grading and image quality estimation challenge. *Patterns*, page 100512, 2022. 7
- [22] Xiao Liu, Pedro Sanchez, Spyridon Thermos, Alison Q O’Neil, and Sotirios A Tsaftaris. Learning disentangled representations in the imaging domain. *Medical Image Analysis*, 80:102516, 2022. 1
- [23] Lucas Mansilla, Rodrigo Echeveste, Diego H Milone, and Enzo Ferrante. Domain generalization via gradient surgery. In *Proceedings of the IEEE/CVF international conference on computer vision*, pages 6630–6638, 2021. 8
- [24] Angus Nicolson, Lisa Schut, Alison Noble, and Yarin Gal. Explaining explainability: Recommendations for effective use of concept activation vectors. *Transactions on Machine Learning Research*, 2025. 2
- [25] Tuomas Oikarinen, Subhro Das, Lam M Nguyen, and Tsui-Wei Weng. Label-free concept bottleneck models. *arXiv preprint arXiv:2304.06129*, 2023. 3
- [26] Frederik Pahde, Maximilian Dreyer, Leander Weber, Moritz Weckbecker, Christopher J. Anders, Thomas Wiegand, Wojciech Samek, and Sebastian Lapuschkin. Navigating neural space: Revisiting concept activation vectors to overcome directional divergence, 2024. 2, 4
- [27] Prasanna Porwal, Samiksha Pachade, Ravi Kamble, Manesh Kokare, Girish Deshmukh, Vivek Sahasrabudhe, and Fabrice Meriaudeau. Indian diabetic retinopathy image dataset (idrid): a database for diabetic retinopathy screening research. *Data*, 3(3):25, 2018. 7
- [28] Connor Shorten and Taghi M Khoshgoftaar. A survey on image data augmentation for deep learning. *Journal of big data*, 6(1):1–48, 2019. 1
- [29] Susu Sun, Lisa M Koch, and Christian F Baumgartner. Right for the wrong reason: can interpretable ml techniques detect spurious correlations? In *International Conference on Medical Image Computing and Computer-Assisted Intervention*, pages 425–434. Springer, 2023. 1
- [30] Rohan Taori, Achal Dave, Vaishaal Shankar, Nicholas Carlini, Benjamin Recht, and Ludwig Schmidt. Measuring ro-

bustness to natural distribution shifts in image classification. *Advances in Neural Information Processing Systems*, 33:18583–18599, 2020. [1](#)

- [31] Qijie Wei, Xirong Li, Weihong Yu, Xiao Zhang, Yongpeng Zhang, Bojie Hu, Bin Mo, Di Gong, Ning Chen, Dayong Ding, et al. Learn to segment retinal lesions and beyond. In *2020 25th International Conference on Pattern Recognition (ICPR)*, pages 7403–7410. IEEE, 2021. [7](#)
- [32] Jee Seok Yoon, Kwanseok Oh, Yooseung Shin, Maciej A Mazurowski, and Heung-II Suk. Domain generalization for medical image analysis: A survey. *arXiv preprint arXiv:2310.08598*, 2023. [1](#)
- [33] Mert Yuksekgonul, Maggie Wang, and James Zou. Post-hoc concept bottleneck models. *arXiv preprint arXiv:2205.15480*, 2022. [2](#), [6](#)
- [34] Yi Zhou, Boyang Wang, Lei Huang, Shanshan Cui, and Ling Shao. A benchmark for studying diabetic retinopathy: Segmentation, grading, and transferability. *IEEE Transactions on Medical Imaging*, 40(3):818–828, 2021. [6](#)

A. Diabetic Retinopathy Concept Creation

For creating images representing diagnostically relevant concepts, we use the pixel-wise annotations of the FGADR dataset to construct positive and negative concepts. An illustration of concept overlap in the fundus images, motivating the need for a controlled creation pipeline, is provided in Figure 8.

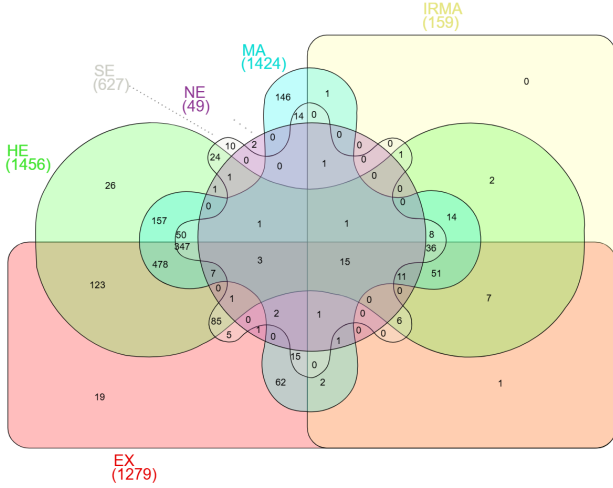


Figure 8. Concept entanglement diagram for FGADR dataset, showcasing how often all concepts coincide in a single image.

First, we horizontally flip all left-eye images to ensure consistent orientation across the dataset, so that all eyes appear as right-eye views. This will not introduce bias, as all training images can be randomly flipped.

For creating backgrounds, we start with defining the set of healthy images. We take all images that do not have any lesion annotations. Then, a subjective visual assessment is made to exclude healthy images with irregular patterns. Although possibly introducing bias, this is done to ensure the remaining candidates can serve as a background that does not introduce much noise.

After these steps, we apply the concept creation pipeline to create 128 positive and negative concept image pairs. This was a trade-off decision: while more concepts would always be preferable for creating stable LCRs, increasing the number would require reusing source images more often, reducing variability across concept examples. Note that the number of 128 could be sufficient, as natural images only need a couple dozen images [15]. An example of such a pair is shown in Figure 9.

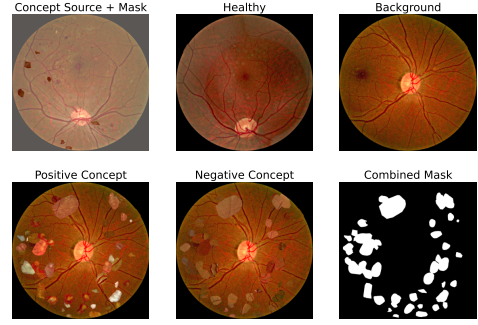


Figure 9. Example of concept creation pipeline on the fundus images from the FGADR dataset for concept: *Soft Exudates*. Done on non-preprocessed data for visualisation, as patches can be seen more easily without correcting for colour.

Internal Consistency and Domain Robustness. We conducted experiments to evaluate whether using multiple source images per concept pair improves the quality of the learnt LCRs. Results of these experiments are shown in Figure 10. To this end, we measured the accuracy of the internal DB of filter-CAVs, computed across all layers of a ResNet50 trained on the APTOS dataset.

While high DB scores indicate that positive and negative concept examples are well-separated in the latent space, this alone does not confirm that the resulting LCRs are meaningful. Rather, it provides a necessary, but not sufficient, condition for their utility in LCRReg. If the concepts were not consistently separable, the resulting DBs and CAVs would be no more informative than random directions in the representation space.

In addition, we evaluated the CAVs on a model trained on the FGADR dataset, the same dataset from which the concepts were derived. This experiment was conducted to assess whether concept performance improves significantly when evaluated in-domain. If performance on the FGADR-trained model is not substantially higher than on a model trained on APTOS, this suggests that the concepts are robust to data shift, as their utility does not strongly depend on the training domain of the model.

Results. We found that using only a single source image per concept pair resulted in near-random DB scores, indicating poor separability in the latent space. Increasing the number of source images improved performance: using five images led to substantially better results, and using ten yielded further improvements. We did not extend beyond ten images due to limited data availability and the need to preserve variability across concept examples. DB accuracies were comparable between models trained on APTOS

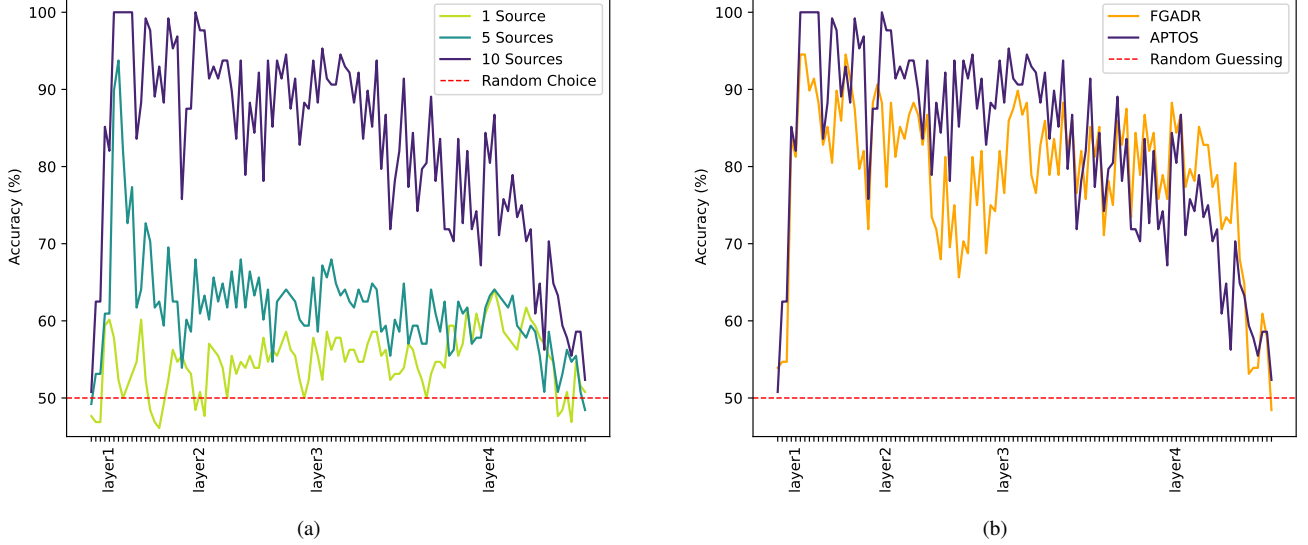


Figure 10. Illustrations of the internal coherence score per layer of a ResNet50 trained on APTOS. Filter-CAV was calculated using 128 images, and evaluated using 64 other images, using accuracy of the internal decision boundary. The train-test split was created using different source images. (a) shows the relation between number of source images per concept example, while (b) depicts the effect of changing the models' training data.

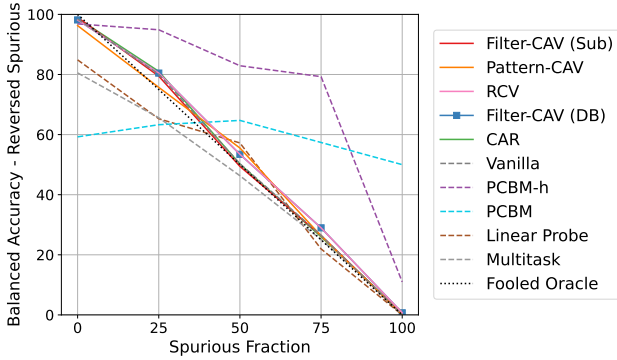


Figure 11. Performance averaged over 5 runs of various LCRReg models, PCBM-h, and the vanilla model, assessed across multiple values of p_{SC} . Models are using hyperparameters that are tuned using Optuna, with the validation set being of similar distribution as the training set.

and FGADR, suggesting that the learnt concepts are robust to data shift and do not rely heavily on the training domain.

B. Ablations

In this Appendix, we report further results of ablations studies. In particular, Figure 12 and Figure 13 show additional ablations on hyperparameters and training strategies on the Elements dataset, discussed in Section 3.1. Table 2 shows performance of LCRReg on different model architectures, which is addressed in Section 3.2.3.

C. Robustness to Spurious Correlations

Figure 11 reports the results of the different models on the APTOS dataset with the hyperparameters finetuned with Optuna, commented in Section 3.2.1. Note that we also provide the accuracy of PCBM, which is equal to PCBM-h without residual fitting. However, this is not discussed in the main section due to it not achieving performance significantly different than random performance, and it is thus not reported in Figure 6 in the Main Text.

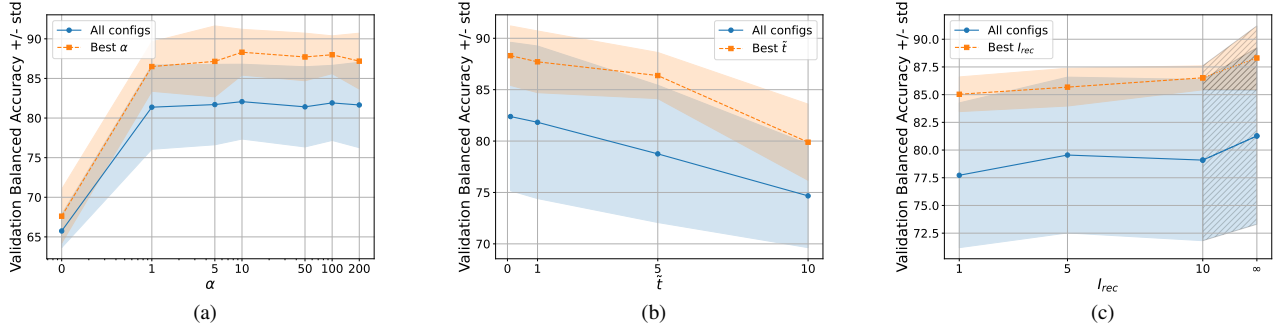


Figure 12. Results of hyperparameter grid search on the binary classification task (Elements dataset) using filter-CAV with cosine loss. Each configuration was run five times with different train/validation splits. Blue lines: mean \pm std over all combinations of remaining parameters. Orange lines: mean \pm std with best setting of other parameters per fixed value. (a) Weight of the \mathcal{L}_{CRRReg} : α_t . (b) Starting epoch: \tilde{t} . (c) Recomputation interval: I_{rec} .

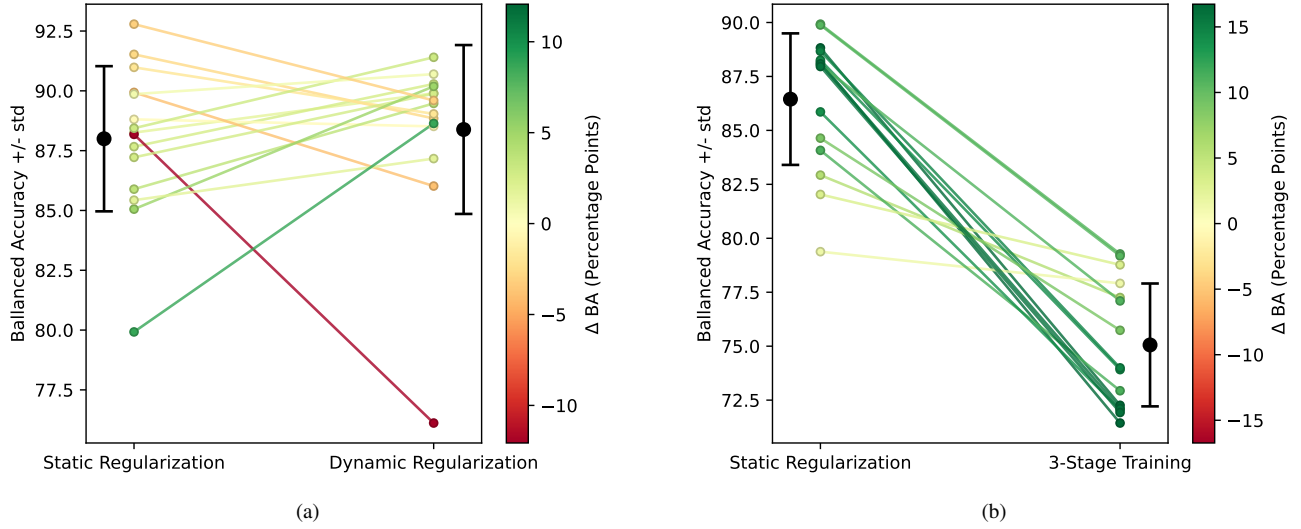


Figure 13. Comparison of different Static regularisation to both Dynamic regularisation, and 3-Stage Training, evaluating all approaches on 15 distinct train-test dataset pairs. The figure shows both the Balanced Accuracy (BA) of individual runs, and the total average. Statistical comparison was done via pairwise t-testing. Comparison of Static regularisation vs. (a) Dynamic regularisation and vs. (b) 3-Stage Training.

Table 2. Performance of Latent Concept Representation-based regularisation across different datasets and model architectures, trained and evaluated on APTOS. Trained on a Spurious Dataset with $p_{SC} = 1$. Performance reported in terms of balanced accuracy. Parameter counts (in millions) are shown in parentheses below model names.

Dataset	Model	ResNet18 (11.6 M)	ResNet152 (60.2 M)	DenseNet121 (8.0 M)	InceptionV3 (23.9 M)
Reverse Spurious	Vanilla	14.81 (9.87)	14.60 (9.76)	43.71 (13.10)	17.96 (4.32)
	Regularised	31.47 (15.55)	16.82 (16.07)	65.74 (11.83)	49.12 (6.27)
Base	Vanilla	75.32 (5.70)	84.81 (6.16)	88.91 (4.15)	79.66 (6.16)
	Regularised	80.14 (5.72)	82.32 (1.56)	85.26 (2.42)	66.25 (9.80)
Spurious	Vanilla	99.69 (0.23)	99.66 (0.26)	99.06 (0.50)	97.22 (1.47)
	Regularised	99.49 (0.30)	99.32 (0.86)	93.78 (3.58)	80.49 (12.0)